Thermochimica Acta, 203 (1992) 419–444
Elsevier Science Publishers B.V., Amsterdam

Martensitic transformations in shape-memory alloys. Successes and failures of thermal analysis and calorimetry

V. Torra [a] and H. Tachoire [b]

[a] *Applied Physics Department, ETSECCIP, UPC, Jordi Girona Salgado 31, E-08034 Barcelona (Spain)*
[b] *Thermochemistry Laboratory, University of Provence (Aix-Marseille I), Place Victor Hugo, F-13331 Marseille Cedex 03 (France)*

(Received 28 August 1991)

Abstract

The development of adapted equipment for high-resolution thermal analysis (thermomicroscopy, acoustic emission, stress–strain and heat conduction calorimetry) provides macroscopically relevant information about the microscopic interactions and the effect of the defects in martensitic transformations of Cu-based shape-memory alloys, e.g., levels of resolution and evolution time scales, intrinsic thermoelasticity, separation between the effects of nucleation and friction. Furthermore, making direct measurements and applying a simple thermodynamic formulation directly relates the friction work (mechanical, analogous to the entropy production) with the width of the calorimetrically calculated hysteresis cycle. Thus, some thermodynamic difficulties found in the measurements and encountered in recent interpretations in the literature are avoided.

INTRODUCTION

In metal alloys, in Ni–Ti (nitinol), copper- or iron-based, in organic materials (queratine) or plastics, in ion crystals, etc., a martensitic transformation appears which is crystallographically reversible. Practical interest in the transformation is associated with its complete recovery when retransformation is made. For this, it is only necessary to reverse the mechanical or thermal action (mechanical stress or cooling) which induces direct transformation. The particular behaviour of the material is associated with the existence of a first-order martensitic transformation without diffusion, called thermoelastic, between two metastable phases. The austenite phase (parent phase) is obtained by quenching from its region of stable existence.

Correspondence to: V. Torra, Applied Physics Department, ETSECCIP, UPC, Jordi Girona Salgado 31, E-08034 Barcelona, Spain.
Dedicated to Professor Joseph H. Flynn in honour of his 70th birthday.

For example in the case of alloys of Cu–Zn–Al, a body-centred cube (bcc) phase, frozen by quenching from the region of temperatures between 500 and 850°C, is converted into a face-centred tetragonal phase (fct), which is somewhat monoclinic, when it undergoes martensitic transformation (see refs. 1–7 and related references).

The phase change is accompanied by a relatively small volume change (from β to martensite, $\Delta V/V \approx -0.08$ in Cu–Zn–Al 18R [8]) and the phenomenological interpretation of the transformation is made from the dilations and contractions of the axes of the crystal, together with an appropriate shear. The positions of the various atoms of the crystal involve the participation of several atomic layers in the elemental cell. In this way, martensites 2H (hexagonal), 3R, 6R, 9R and 18R appear. The crystallographic characteristics and phenomenological mechanisms of transformation are known for standard materials, and relevant data can be found in the bibliography.

The industrial applications of memory alloys (shape-memory alloys) are associated with the possibility of "educating" or training the material. This makes it possible to have two forms: "hot" or austenite, and "cold" or martensite. Furthermore, there is a mechanical force associated with the heating process (up to 70 kp mm^{-2}), when passing from the cold form to the hot form. The applications are associated with the construction of an indicator which is activated by a slight change in temperature. In fact, a few degrees are sufficient to pass from one phase to the other. From the transformation characteristics, the construction of "micromotors" may be considered, which would produce a progressive stress in relation to the temperature. In particular, the macroscopic thermoelasticity or pseudo-elastic effect involving the relation between stress, strain and temperature, establishes that a continuous stress field is present depending on the values of temperature and deformation.

The particular behavioural features of this type of material during transformation have found a restricted area of application as actuators. Its properties are equivalent to those of systems made up of elements currently available: thermometric sensors, stepper motors, springs and in complement, operational electronics and its batteries. Their replacement by a single device, operated by an alloy, is very interesting, particularly in aggressive environments. In fact, electronic equipment is very sensitive to the action of ionising radiation. It is unable to work in electromagnetic or particle fields.

Temperature control systems are available on the market that are based on memory alloys of Cu–Zn–Al and which can be used a limited number of times. Thus, connection systems are built in avionics and prototypes of heat engines have been built which use small differences in temperature for the development of replacement energy sources. But their use as custom-built parts in standard equipment (car industry, home computer

connection systems, etc.) involves having a high economic competitiveness together with a remarkable reproducibility and high behavioural reliability. For example, from the two memory effect, tens of thousands of complete working cycles (austenite/martensite) in two to five years are expected. In this sense, it is also necessary to have predictable knowledge of the surface of state (stress, strain, temperature), such that the material will not degrade with time (ageing, fatigue) any more than the materials currently used and that it will be much more economical.

Experimental analyses of the behaviour of the alloys [9,10] (hysteresis cycles, diagrams of stress, strain and temperature) have revealed the importance of atomic order, of defects (dislocations, precipitation), of the size of the grains in the polycrystals [11], of the effects of the surface state, etc., on the macroscopic characteristics of the material. In particular, the actions of repetitive thermomechanical treatments (cycling) produce material ageing and fatigue. This tells us that the microscopic state and its evolution have a great influence on the macroscopic behaviour and, as a result, on the "thermodynamic equation of state". Given the industrial interest in having a quantitative form of the equation of state, it will be necessary to include in it the structural parameters. All this involves having comparative, global and local analyses of the transformation, and systematized phenomenological information.

In recent years, a set of data, frequently contradictory, complementary or irrelevant (see, for instance in ref. 12, how the increase in M_s after quenching is explained by an isothermal transformation mechanism), have progressively described in detail, by means of macroscopic measurements, the behaviour of the material. Acquiring the measurements has required the development of adapted instrumentation. New equipment has produced results which required new interpretations in structural terms. Frequently the microscopic effects are very slight and very difficult to detect with standard characterization techniques (TEM, X-rays). In fact, causal and clearly visible changes in some degrees or tenths of a degree in the characteristic transformation temperatures, which in some cases can be associated with atomic evolutions, are practically undetectable by means of crystallographic techniques. Also, the main lines of research, necessary for the systematic and predictive descriptions of material behaviour, have produced a series of papers leading to the formulation of an equation of state [13–20]. In some cases, formulations based on interpretations of the hysteresis cycle from the calorimetric results violate the laws of thermodynamics; for instance, in ref. 21, the efficiency of the thermal cycle (see the cycling processes in Fig. 1 and the energy absorbed/released in Fig. 2 of ref. 21) is ten times the efficiency of the equivalent Carnot cycle.

In this study we present an outline of the systems of high-resolution thermal analysis adapted for studying memory alloys, some examples of their possibilities for detecting small structural evolutions and a simple

thermodynamic analysis of the hysteresis cycles which correctly produces the magnitudes of interest from the calorimetric thermograms.

THE EXPERIMENTAL SET-UP IN HIGH-RESOLUTION THERMAL ANALYSIS (HRTA)

The calorimetric measurements of transformation–retransformation cycles make it possible to establish that, for each type of alloy or composition, the material passes from one phase to another within a region of some tens of degrees and that, for Cu–Zn–Al, the energy released is around 6 J g^{-1}. When samples of around 100 mg (a volume close to 10 mm^3) are used, conventional devices can provide the thermodynamic information which, according to the aims, are sufficient. Commercial DSCs (differential scanning calorimeters) provide a resolution close to 10 μV and have a calorimetric sensitivity of around 200 mV W^{-1}. The resolution in temperature is 0.1 K and the working area extends from the temperature of liquid nitrogen (around 100 K) to 850 K. In DTAs (differential thermal analysers), the sensitivities are lower but the working area may reach or exceed 1500 K, surpassing the melting temperature of the alloys of interest.

The average characteristics of the systems available on the market make it possible to reach a certain level in the study of the materials. The suitability of a given instrument will depend on the type of process required and, where appropriate, on the type of material. When a study is made of a martensitic transformation, phenomena are seen that depend on the type of instrumentation used. In fact, acoustic emission has revealed the complexity of the transformation process. The introduction of heat flux or conduction calorimetry made it possible to establish correlations between the acoustic emission and the thermokinetics of the process. The tests carried out to calculate the correlation established that the complexity of the acoustic emission demands that thermal analyses have an acceptably "equivalent" separating power. This means a resolution in the temperature of the order of (or higher than) 0.01 K. Similarly, calorimetric resolution (heat flux or conduction calorimetry) in the measurement of energy is lower than the possibilities of ultrasound detection. In impulse transformations it is of the order of 25 μJ. Acoustic impulses in the observations of $\beta \rightarrow \beta'$ (Cu–Zn–Al alloys) are situated in a domain between 0.1 and 10^{-7} μJ (resolution limit of the equipment used) [22,23]. Furthermore, experimental analyses have made it possible to establish that both techniques produce complementary information concerning the transformation process. Calorimetrically, the energies associated with the transformed masses are detected, and, acoustically, the release of the interphase pinnings (unpinning processes) or the nucleation processes are detected.

The set of conditions imposed in carrying out the experiment suggests that transformation should be studied so that the phenomena under study

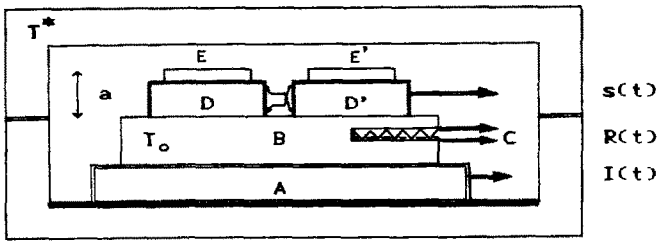

Fig. 1. High-resolution thermal analysis or HRTA, CTT-UPC patent: T^*, temperature of the external thermostat; A, thermobattery (Peltier-effect plate) powered by a programmable current intensity $I(t)$; B, working area made up of a copper plate at temperature $T_0(t)$; C, Pt-100 resistance; a calorimetric system situated in the working space and operating at temperature T_0; D and D′, calorimetric detectors; E and E′, sample and reference.

may be separated. In order to do this, we choose to operate in restricted temperature areas situated close to room temperature. The basic aim is to have rigorous control and automation that is easy to perform. With these limitations, the Peltier effect is very suitable because the cooling/heating processes are performed without difficulty from a programming of the intensity of the Peltier current. The signal processing associated with a systematic modelling of the experimental device makes it possible to compensate for the instrumental effects and to smooth the effect of the noise. The various instruments and devices for high-resolution thermal analysis operate from PC-XT- or 286-AT-type computers by means of programs written in MICROSOFT ASSEMBLER and QUICK-BASIC language.

Figure 1 shows a thermal analysis stage together with adaptations to convert it into a calorimetric system. In this case a thermostat at temperature T^* is used. Temperature control and programming are made from an approximation to the causal ratio between the intensity of the current produced by the Peltier effect and the temperature of the working space. In order to correct the differences between the values predicted and those obtained, a supplementary on-line correction is introduced.

The working space may be used for measuring various parameters. It is possible to follow the thermal analysis with an optical microscope (thermomicroscopy) with a videotape recording system for further study. A mechanical traction device may be built, making it possible to calculate the surface of state, stress (σ), strain (ε) and temperature (T). The electrical resistance of the sample under study may be measured, or the associated acoustic emission may be detected, etc.

In order to have effective programming, it is necessary to know the thermal parameters of the experimental device. This presupposes establishing a minimally representative model of the physical characteristics of the system. With this object, the model based on the transport of heat by conduction used in the representation of the invariant systems (models at

localized constants) may be used. This type of representation provides a set of N linear differential equations ($i = 1, 2, \ldots, N$) of the form

$$W_i(t) = C_i \, dT_i/dt + \sum_{k \neq i} P_{ik}(T_i - T_k) + P_{i*}(T_i - T^*) + P_{i0}(T_i - T_0) \qquad (1)$$

In general, the coefficients are functions of temperature; T^* is the temperature of the external thermostat, T_0 is the temperature of the working stage, and in the $W_i(t)$ model all the Peltier and/or Joule dissipations should be included.

This formulation makes it possible to apply the algorithm AIRRT to Joule or Peltier tests carried out at different constant temperatures [24,25]. From them, for each temperature, an approximation to the physical characteristics of the experimental system can be obtained. In order to make simulations that represent the effect of the temperature programming, it is necessary to use a numerical approximation of the system of differential equations (see, for instance, the Runge–Kutta algorithm). In fact, there are different parameters that evolve with the value T_0.

In the region of low intensities, small temperature variations are obtained and it may be considered that the intensity is proportional to energy dissipation. In these conditions it may be assumed that the system is governed by invariant system equations (models at localized constants). The ratio existing between current intensity and temperature, determined in the Pt-100 resistance from reference values (I_{ref}, R_{ref}) and derived from eqn. (1), takes the form

$$\Delta I + a\frac{d\Delta I}{dt} + b\frac{d^2\Delta I}{dt^2} + \ldots = \frac{1}{S_P}\left[A\frac{d^N\Delta R}{dt^N} + B\frac{d^{N-1}\Delta R}{dt^{N-1}} + \ldots + \Delta R\right] \qquad (2)$$

In the above expression, $\Delta I = I - I_{ref}$, $\Delta R = R - R_{ref}$, S_P is the sensitivity of the Peltier effect and the series of coefficients a, b, ..., and A, B, ... are related to the series of poles ($-1/\tau_i$) and zeros ($-1/\tau_j^*$) of the Transference Function TF(p) which, in the Laplace space, takes the form [26–29]

$$\mathrm{TF(p)} = \frac{1}{S_P}\frac{\prod_{j=1}^{M}(\tau_j^* p + 1)}{\prod_{i=1}^{N}(\tau_i p + 1)} \qquad (3)$$

The experimental study of the system response, for a set of values of T^* and T_0, establishes that S_P depends in a relevant manner on T^* and on the difference between T^* and T_0. However, the evolution of the poles and the zeros is relatively smooth with the temperatures. In this way, for programmings of some tens of degrees, it is possible to consider them constant and equal to their mean values. This permits a semi-quantitative

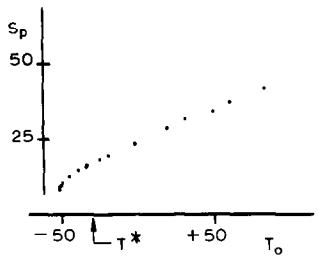

Fig. 2. Sensitivity S_P (K A^{-1}) of the Peltier effect versus the temperature T_0 (°C). The thermal bath temperature $T^* \approx -30.0$°C.

approximation from the same differential equation relating the intensities $\Delta I(t)$ to the resistances $\Delta R(t)$. The series of coefficients a, b, ..., and A, B, ... are kept constant and a variable sensitivity $S_P = S_P(T^*, T_0 - T^*)$ is chosen from a series of calibrations of the Peltier effect (Fig. 2). In order to make calculation easier, these approximate to a rational fraction of the form $P(x)/Q(x)$. If the degree of the numerator is M and that of the denominator is N, Pade's approximant is represented by $\{M, N\}$. For temperatures T^* near to room temperature, the overall form of function S_P is satisfactorily represented by means of a Pade's approximant of the type {3,1}.

In order to ensure coincidence between the values predicted and those obtained during programming, a local correction is carried out from the same model used for performing the first open-loop calculation. The correction uses the same differential equation – from the difference existing between the value predicted and that obtained – and makes a forecast of the actions to be carried out so that, some seconds later, the difference may be cancelled. If the programmings (temperature rate) are made with evolutions of some mΩ s^{-1}, the differences between the programming predicted and that obtained do not exceed ± 0.01 K. The noise associated with the measurements and dynamic characteristics of the system limit the temperature rates which are accessible for a certain programming. These values can be analysed easily if the model (via the transference function TF) is represented in module and frequency coordinates using the Z transform and its subsequent conversion to frequency space (see for instance refs. 30 and 31).

From two thermal analysis stages (29,32–34] a system can be constructed which makes it possible to study the stress–strain–temperature diagram. The system (computer controlled) has the same high resolution in temperature, close to ± 0.01 K, in the region of room temperature (± 1 mΩ is equivalent to ± 2.5 mK). In measuring strain, there is a resolution of ± 0.1 μm (maximum shift = ± 1 mm) and the force is determined with a resolution of ± 1 mN for total loads of less than 20 N [35].

TABLE 1

Working temperature T_0 (in Ω, from the Pt-100) and calorimetric sensitivity S_c (mV W^{-1}) determined from Joule dissipations in steady state. The external thermal bath temperature T^* is −30°C

T_0	S_c	T_0	S_c
79.08	558.0	88.35	628.6
79.18	558.0	88.61	628.7
79.40	560.1	124.25	748.1
79.93	563.9	124.79	757.4
86.63	617.3	133.48	747.3
88.33	628.4		

When semiconductor plates are placed in the working space, there is a heat flux or conduction calorimetric system. In this case, the same base configuration is used [28,29,36–38] that has produced remarkable results for transformation temperatures, entropy production and martensitic transformation thermokinetics, and also (see below) yields results in terms of the energies released. In these "classic" systems, the calorimetric detectors were situated inside small copper blocks which, with a slight thermal protection, were spontaneous cooled or heated directly by means of liquid nitrogen vapour or by means of a heating resistance.

In order to use the calorimetry described in Fig. 1, a suitable calibration of the Seebeck effect should be made by means of the Joule effect (see Table 1). The system is automated [32–34]. In order to calibrate the calorimetric sensitivity S_c, the computer generates voltage impulses which produce the Joule effect when the response to Peltier's effect (cooling or heating) has reached a stationary state. In order to control the efficacy of the calorimetric system during a given programming, Joule signals can be

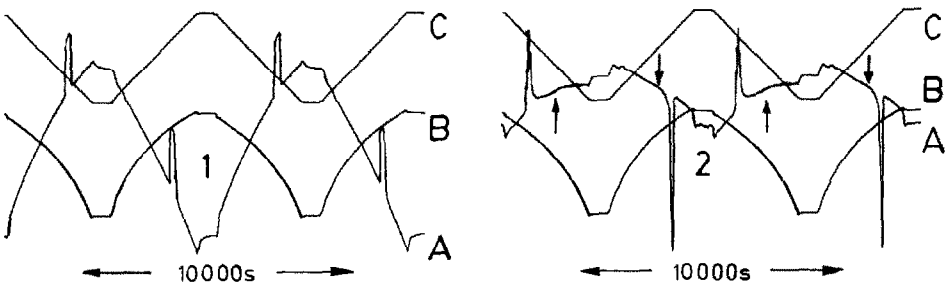

Fig. 3. Experimental calorimetric curves versus time with an automatic cycling between −40°C and +41.7°C: A, calorimetric thermogram; B, Peltier intensity current; C, temperature; in arbitrary units. 1, Joule effects; 2, martensitic transformation; the arrows indicate a slight baseline deformation.

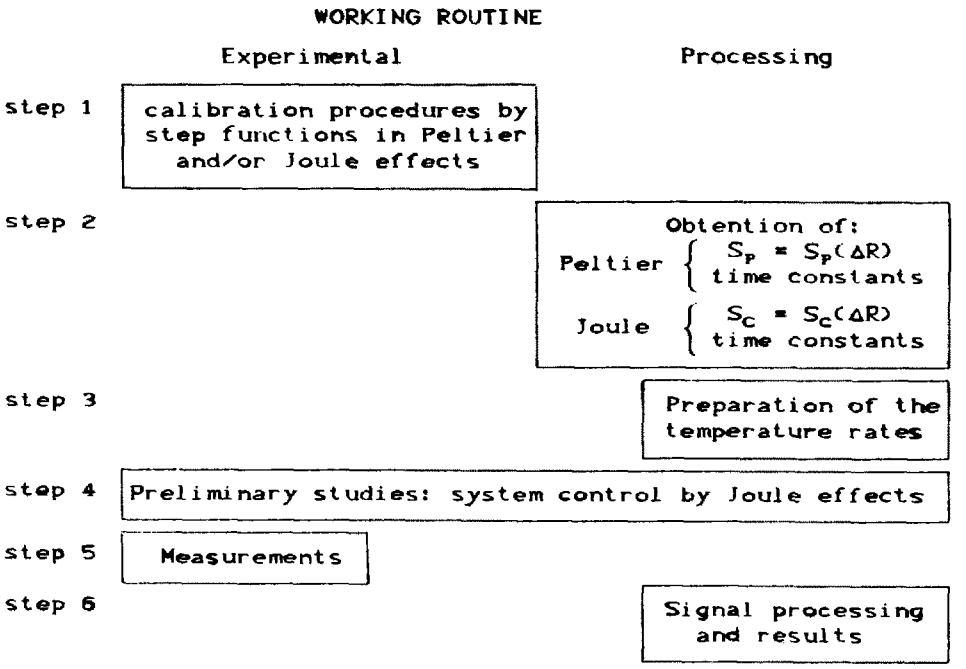

Fig. 4. Flow diagram of the calorimetric routines; in high-resolution thermal analysis the unnecesary steps, i.e. the Joule effects studies in steps 1, 2 and 4, can be avoided.

generated in order to check the reliability of the equipment and of the treatment routines (Fig. 3).

Baseline analysis and the analysis of its connection with the Peltier intensity make it possible to eliminate its effect once a Pade's approximant is obtained which links both evolutions (baseline and Peltier intensity). The thermogram obtained or, where appropriate, an auxiliary signal process in order to compensate the inertia of the detectors, provides the thermodynamic magnitudes of interest (see Fig. 4): in particular, characteristic transformation temperatures, amounts of heat exchanged, an approach to the entropy change by $\int \delta Q/T$, entropy production, hysteresis cycles (Fig. 5), etc.

SUCCESSES IN HIGH-RESOLUTION THERMAL ANALYSIS (HRTA)

Using an HRTA set-up equipped with a system of observation under an Olympus metallographic microscope (type BH2-UMA) and a Sony low-priced recording system (video camera EVC-X10, video cassette recorder SLV353 and TV Trinitron), together with possibilities of acoustic detection (Bruel and Kjaer amplification system), of measuring electrical resistance and of manually exerting a low mechanical stress, some experimental observations have been made.

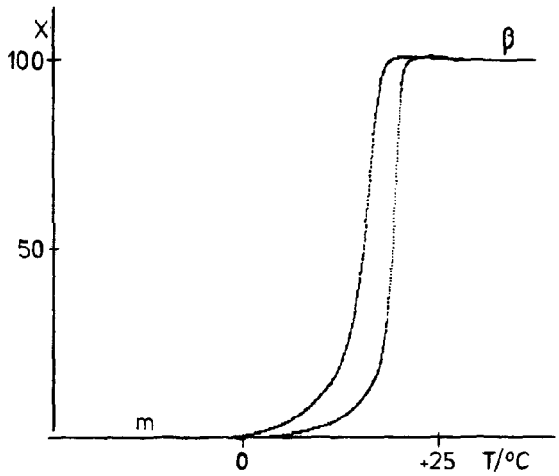

Fig. 5. Hysteretic behaviour of transformation–retransformation processes obtained from accumulated enthalpy (thermogram in Fig. 3B); X (% β-phase) versus temperature.

(1) The connection between acoustic emission and shifts or sudden appearances (burst movements) of the interfaces [39].

When the high sensitivity of acoustic emission (AE) was coupled with HRTA, the observations connected the accelerations in the interfaces movement with the appearance of AE. Therefore, the diverging interpretations between the resistance measured and the AE observed [40] and the existence of invisible nuclei [41] are questionable.

(2) A complete reproducibility of the behaviour for successive thermal cycles which produces equal acoustic pulses for the same temperatures [22,42,43].

The problems of stochasticity associated with transformation are probably associated with the evolution of the material (atomic order versus time and the dislocations created by burst transformations) and with the uncertainties concerning the external control parameters, e.g. the temperature and/or stress control and temperature rate and/or stress rate.

(3) An evolution of the M_s with time from the initial quenching by an evolution of the different atomic order parameters (B_2 and/or $L2_1$ in Cu–Zn–Al 18R transformation). This depends on the type of initial heat treatment, on the coexistence of both phases and on the processes of martensite stabilization and recovery of the beta phase [44–47].

The analysis of the behaviour of an interphase β to martensite with temperature and/or time makes it possible to examine in detail, where appropriate, the separate different perturbing effects. This helps to distinguish the various microscopic mechanisms involved and, where appropriate, to correlate them. In a simplistic way, they might be associated only with "stochastic perturbations in the material". Figure 6 (from ref. 48)

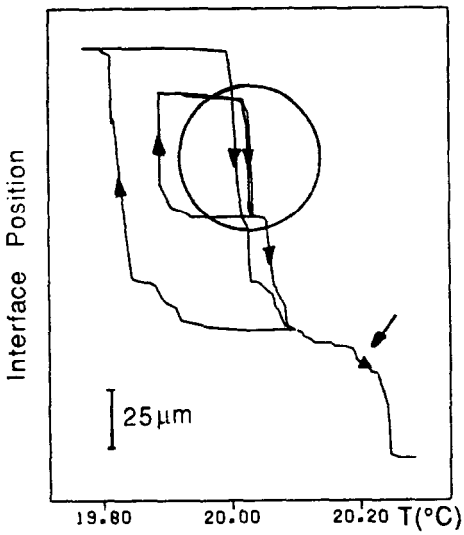

Fig. 6. Partial hysteretic behaviour in a single, stress-free, martensite plate (air-quenched sample). Plate width versus temperature; the position of the "internal" cycle (see circled zone) is connected with the changes in transformation temperatures with elapsed time (from ref. 48). The slope (dx/dT, see arrows) shows the action of the intrinsic thermoelasticity; right arrow: increasing temperature is necessary to induce the retransformation in a "gentle" stabilized martensite.

shows a partial transformation–retransformation cycle which is partially outside a larger cycle. The shift occurs as a result of opposing influences on local temperatures of transformation with the permanence in martensite (stabilization) or in the beta phase (recovery). The m-stabilization [49–52] produces an increase in transformation temperatures and the β-recovery produces a "recovery" to the standard values.

(4) The existence of an intrinsic thermoelasticity (see Figs. 6–8) associated with the concentration of dislocations of the material due to the progressive creation of stacking faults with the movement of the interphases in the martensite growth [53].

The intrinsic thermoelasticity makes a progressive cooling (or an increase in mechanical stress) necessary in order to increase the amount of martensite. Thus, it stimulates the spontaneous nucleation of other martensite plates. Industrial materials contain a high concentration of dislocations during to the quenching necessary to freeze the parent phase. Therefore, and in the absence of evolution (atomic order or dislocation creation), the intrinsic thermoelasticity together with nucleation of the new martensite plates control the forms of partial or overall transformation–retransformation hysteresis cycles.

(5) The spontaneous nucleation of the second beta phase [54] in particularly remarkable crystallographic situations suggests a somewhat clearer

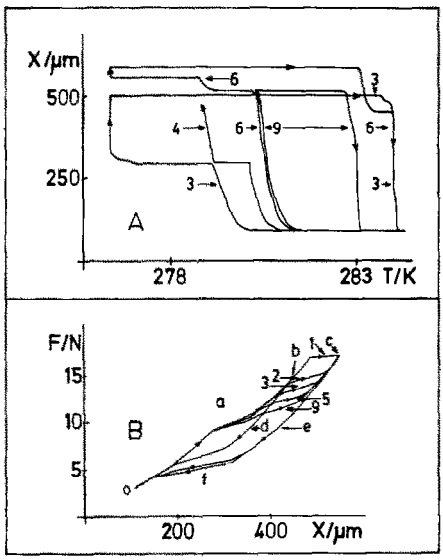

Fig. 7. Hysteretic behaviour of the single martensite plate. Sample: Cu–Zn–Al with γ precipitates (diameter approx. 100 Å). (A) Temperature-induced transformation (cycles 3, 4, 6 and 9); values of the η_{th} slope dx/dT in cycle 9 are consistent with thermoelasticity in air-quenched samples. (B) Stress-induced transformation without nucleation processes (growing/shrinking only); oabdo, previously cycled zoned, maximum force (F_b) at point b; oacefo, increased zone (cycles 1, 2, 3, 5, 9), maximum force (F_c) at point c; the slopes (a and f zones) in cycle 9 are consistent with the intrinsic thermoelasticity.

interpretation of the existence of the memory effect. When a single martensite domain reaches one end of a sample, it may nucleate the second beta phase producing the breakdown of the shape-memory effect (SME).

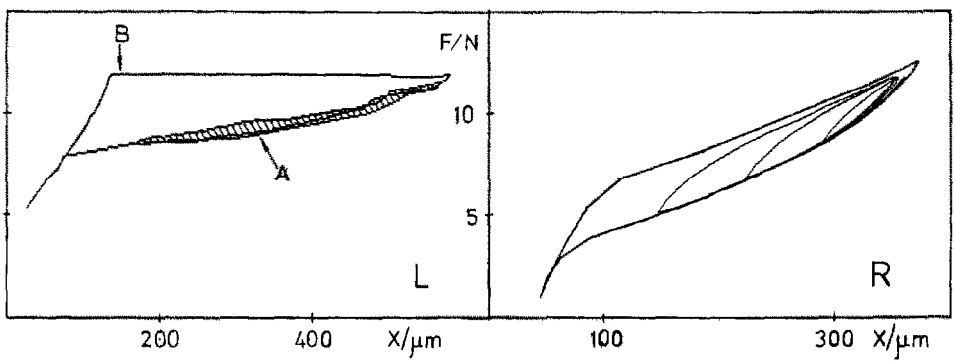

Fig. 8. Force versus increased length in high-resolution stress–strain observations. (L) Air-quenched sample: A, single interface friction phenomena without nucleation; the friction work in the hatched zone is 170 μJ; the slope df/dx relates to the intrinsic thermoelasticity; B, single interface nucleation processes. (R) Water-quenched sample: repetitive cycling with N martensite plates ($10 < N < 50$).

Second beta-phase nucleation only appears in perfect single crystals of martensite.

This possibility indicates that reversion to the same "normal" form (the memory effect) is the normal retransformation process. In a transformation with several variants, these are only crystallographically coherent with the initial phase. When a "standard single crystal" of martensite is produced, the defects existing in the areas of coalescence (the intrinsic thermoelasticity which is coupled with the concentration of dislocations assists in the nucleation of martensite in different domains) bring about the reappearance of the initial beta phase and, as a result, of the memory effect. Only a low dislocation concentration in the sample can bring about the breakdown of SME.

(6) The remarkable evolutions of the first transformation cycles (Cu–Zn–Al) when an analysis is made of the behaviour of a martensite domain under the action of a cyclic programming of the temperature when it contains small type-γ precipitates (diameter ≈ 100 Å).

Thermomicroscopy establishes the existence of a very considerable reduction in the width of the hysteresis cycle with the number of cycles. After the first cycle it is reduced by around 30% and after 10 cycles by around 70%. The change is associated with the increase in the M_s temperature and a slight decrease in A_f. Similar results are obtained with stress-induced transformation (see in Figs. 7(A) and 7(B) the temperature and stress changes with cycling); they presuppose the appearance of a privileged direction over the precipitates and, also, an increased thermodynamic stability for the specific martensite variant. These modifications cannot be seen by means of standard calorimetric techniques. In spontaneous transformation, the nucleation of new martensite plates renders the growing/shrinking effects irrelevant.

SOME FAILURES IN SHAPE-MEMORY ALLOYS: FRICTION PROCESSES, ENTROPY PRODUCTION AND THERMODYNAMICS

The hysteresis cycle may be obtained from the energies that provide the calorimetric thermogram, e.g. the accumulated enthalpy versus temperature (Fig. 5). Then, a model of the behaviour of the material is required in order to obtain some of its intrinsic properties from the thermal magnitudes, e.g. the friction energy or the elastic contributions associated with transformation. The information generally provided by the literature from calorimetric measurements appear not to distinguish sufficiently mechanical actions (stress-induced transformations) from thermal actions (temperature-induced transformations). In this latter case, transformation occurs spontaneously under the effect of temperature, and free of external stresses ($\vec{f}_{ext} = \vec{0}$). In this sense the mechanical friction energy $\oint \vec{f}_{ext}\, d\vec{l}e$ is zero. In

TABLE 2

Heat released (A), heat absorbed from calorimetric measurements (B) and friction work (C) in J mol^{-1} M_s, M_1, A_s and A_f transformation temperatures (K); * indicates results opposed to the second law of thermodynamics; η_{th} (%) calculated from experimental data (if available)

A	B	C	M_s	M_f	A_s	A_f		η_{th}	Ref.	Observations
100	25	2	246	244	244	252	*	2.4	21	
210	130	6	246	238	238	252	*	2.5	21	Data from Figs. 1 and 2
340	340	13	246	225	232	252	*	2.5	21	
310	310	6	260	250	255	265		1.9	61	Quenching at 700 K
420	420	7	262	240	245	266		1.9	62	
320	320	12	250	225	235	255	*	3.2	62	Samples with γ
150	150	97	225	–	–	285	*	21	62	precipitates

stress-induced transformation, the friction energy is the net heat released in a complete cycle.

The hypotheses applied in the literature include

(a) The energy dissipation obtained by calorimetry in transformation or retransformation may only be identified with the change in chemical enthalpy if there is no storage of elastic energy. That is, it is only strictly related when the transformations are made by means of a free interphase and without external mechanical stresses [55].

(b) The total thermal energy measured in a complete calorimetric cycle (assuming that there are no relevant changes in specific heat between the two phases) represents the dissipation processes or the friction work [21,56–60].

(c) Using an entropic balance in the hypothesis of zero entropy production requires compensatory work [57]. This condition appears in order to translate the width of the hysteresis cycle in terms of the amount of total heat exchanged ΣQ_i, i.e. as if the material is the fluid operating in a reversible thermal machine (the more elementary machine is the Carnot machine). The value of ΣQ_i, measured from the thermograms of Cu–Zn–Al, is frequently positive (heat absorbed). It has been assumed that this energy leaves the material in the form of an acoustic emission [21,57] (see Table 2).

In some cases, the arguments above were applied to sets of experimental results. The situation becomes remarkably complicated when operating with materials previously submitted to many cycles of education and/or fatigue [63–67]. Also, the application of this kind of model could lead to notable difficulties from the thermodynamic point of view. In fact, when partial cycles are made, increased energy differences appear (even higher than 50%) for hysteresis cycle widths of around 5 K and working temperatures around 245 K. These differences cannot be associated with work

TABLE 3

Calorimetric measurements (J) in Cu–Zn–Al $\beta \rightarrow 2H$ (from ref. 68); e.c., electronic concentration; composition in at.%; A, parent phase to martensite; B, martensite to parent phase; *C*, mean value; *D*, standard deviation; *N* number of measurements

	Sample J1			Sample I1			Sample K2		
	e.c.	Zn	Al	e.c.	Zn	Al	e.c.	Zn	Al
	1.534	8.39	22.52	1.534	13.12	20.13	1.534	6.41	23.51
	A	B		A	B		A	B	
C	−1.288	1.262		−1.60	1.68		−1.67	1.68	
D	±0.008	±0.004		±0.02	±0.02		±0.03	±0.03	
N	8	6		4	5		4	6	

which the material provides on the outside. The performance of a thermal machine operating in this region is 2%. Obviously, the thermodynamic formulation used in ref. 21 and related references is wrong. The * in Table 2 indicates erroneous values.

Also, the calorimetric measurements made for electronic concentrations above 1.40 ($\beta \rightarrow \gamma'$ transformations) suggest that the basic ideas deduced from the measurements on $\beta \rightarrow \beta'$ are insufficient. The hypothesis of "null entropy production" is, obviously, incorrect. Hysteretic behaviour is strictly connected to the entropy production: in stress-induced transformation from work lost or, in temperature-induced transformation, from degraded heat. The acoustic emissions in this transformation ($\beta \rightarrow \gamma'$) are very intense (they are burst-like transformations). By contrast the energy averages are almost equal and within the margin of experimental uncertainty (see in Table 3 some values obtained from ref. 68). This indicates that the interpretation, based on experimental information, is also related to an erroneous evaluation of the thermograms used to describe the thermokinetics of the transformation. This becomes an incorrect choice of base line for the energy evaluation or undefined states of the samples [25].

Working hypothesis

When an analysis is made of the behaviour of the hysteresis cycle of a material, a series of calorimetric measurements are made associated with a set of complete, repetitive heat cycles (to avoid more difficult baseline problems). The sample passes successively from one phase to the other

$$\beta \rightarrow m \rightarrow \beta \rightarrow m \rightarrow \beta \rightarrow m \ldots$$

and we assume that, for each each complete cycle, the same states of the material (initial state I and final state F) are recovered

$$I \rightarrow F \rightarrow I \rightarrow F \rightarrow I \rightarrow F \ldots$$

In order to obtain a model of the behaviour, it has been assumed that the material does not evolve when it has made around 20 cycles. Reproducibility is confirmed when a series of repetitive cycles of elemental transformations SISMP (single interface–single martensite plate) are observed by means of thermomicroscopy and thermosonimetry [22,32,39] but, in spontaneous temperature-induced transformation, there is a marked evolution in the calorimetric thermograms with cycling and a progressive increase in the concentration of dislocations which has been determined at least up to cycle 200 [73].

If we assume that the material does not evolve with cycling, the state functions should recover their values. For internal energy or enthalpy, we can write

$$\oint \mathrm{d}U = 0 \qquad \oint \mathrm{d}H = 0 \tag{4}$$

The experimental situation of the calorimetric observations suggests that in a complete cycle no external mechanical work is done, because the material is not connected with any external mechanical system. In the absence of sensor systems and external stresses, we should consider that the total work exchanged is zero. That is

$$\oint \delta W = 0 \tag{5}$$

Application of the first principle of thermodynamics tells us that

$$\oint \delta Q = 0 \tag{6}$$

If the heat capacities are equal ($c_\beta = c_\mathrm{m}$), eqn. (6) reads $\Sigma Q_i = 0$ or $|Q_{\beta\to\mathrm{m}}| = |Q_{\mathrm{m}\to\beta}|$. In any event, there are sets of results measured by different laboratories using similar devices which provide slightly different values between the processes of transformation and retransformation. If there is a systematic divergence between experimental reality ($\Sigma Q_i \neq 0$) and the energy formulation ($\Sigma Q_i = 0$) it should be completely clarified. Thus, it is possible to consider two alternatives. In the first, an evaluation has to be made of the uncertainties of behaviour of the experimental devices when they are used at variable temperatures. Divergences could arise from the evolution of calibration in dynamic situations ($\mathrm{d}T/\mathrm{d}t \neq 0$) or from the uncertainties linked to the baseline. The second alternative is associated with the lack of knowledge concerning the set of energy processes undergone in the sample. Other alternatives could be considered: reformulation of the thermodynamics applied to transformations, i.e. the first and second laws of thermodynamics, or an assumption that there is an internal and progressive accumulation of energy within the material during hundreds or thousands of cycles.

Thermodynamic and phenomenological analysis

In order to clarify transformation phenomenology, it seems appropriate to make direct measurements of the friction work and, in any event, to

observe the most elementary phenomena possible and compare them with the overall transformations. To do this, we made partial transformations involving the appearance and disappearance and/or the growing/shrinking of a single martensite domain. From a high resolution stress–strain system the result is that the work per cycle that must be supplied is 0.005 J g^{-1}; see zone A in Fig. 8 (left), the stress–strain representation for air-quenched samples. When nucleation has to be included (see zone B in Fig. 8), the friction work is around 0.03 J g^{-1}. When water-quenched samples are used, the results are similar but usually N martensite plates ($10 < N < 50$) are studied with included nucleation (see Fig. 8, right). This tells us that, in a monovariant transformation, the friction energy is less than 1% of the thermal energy released during transformation (near 6 J g^{-1}). That is, even if ΣQ_i represented friction energy (erroneous hypothesis), it would remain below the calorimetric resolution available (near 1%) when we measure the global energy obtained in the transformation.

Detailed analysis of the thermograms associated with the processes of transformation–retransformation of a single plate of martensite indicates that the classical calculation of the baseline is not sufficient. There appear to be metastabilities that affect the "whole" sample and that deform the baseline. A similar behaviour appears for the overall spontaneous transformations. The thermograms associated with overall programmings show slight deformation (see the arrow in Fig. 3) for the range of temperatures below A_s. It is clear that calculation of the baseline is decisive for measuring energy or $\int \delta Q/T$, in particular, in zones with very weak and long-lasting dissipations. Careful calculations of the energy contributions, together with structural techniques, are necessary to understand the complexity of the phenomenology associated with transformation. In any event, it is important to note that conduction calorimetry is as well adapted to measure the dissipations made at "constant temperature", as those associated with first-order transitions, with mixing processes, and with chemical reactions. By contrast, modifications of heat capacity only, introduce baseline evolutions [25,69–72]. Because their internal phenomenology is dependent on the thermoelasticity effects, martensite transformations are made under the action of the changes in temperature and, therefore, can be interpreted as "abnormalities" in the heat capacity.

In general, the material evolves with time and cycling. After an air quenching, the initial concentration of defects is very small and nucleation is difficult. This produces burst-like transformations with a progressive increase in the concentration of dislocations in relation to the number of cycles. Transformation occurs more gently and extends into a wide range of temperatures (temperature extension increased). The existence, on the thermogram, of burst-like transformations and their progressive evolution makes it possible to introduce an entropy production associated with these pulses. In this way, the total entropy production (ΔS_U) can be separated

into two parts: firstly, ΔS_U^b, associated with discontinuous contributions (b or burst) with an evolutionary character [29,34,48]; and secondly, ΔS_U^s, associated with the width of the hysteresis cycle (s or standard) and little affected by the evolution of the sample.

A treatment by signal processing of the thermogram associated with the jth cycle makes it possible to display the pulses more easily and to calculate $\Delta S_U^b(j)$ from

$$\Delta S_U^b(j) = \sum_i \Delta S_{U_i}^b(j) = \sum_{T=M_s}^{T=M_f} m_i c\left[\log(T/(T+\Delta T)) + \Delta T/T\right] \tag{7}$$

The above expression relates to the increase in universal entropy associated with a series of elemental (burst) transformations between M_s and M_f. For this, it is assumed that a material domain of mass m_i undergoes a burst transformation. The energy released in a pseudo-adiabatic form, changes the temperature of the material locally (in m_i) into ΔT (for instance, 4 K which is equivalent to half a hysteresis width). The energy is transferred progressively to the rest of the sample and to the temperature control system (external thermal bath), which are at temperature T. The values of $\Delta S_U^b(j)$ (the jth cycle) obtained from an air quenching, decrease with the number of cycles to a constant value $\Delta S_U^b(\infty)$ (the ∞th cycle) in the "steady state" (see Fig. 9). The change in ΔS_U^b may be associated with the changes inside the material via a "driving force"

$$\bar{T}\Delta S = \bar{T}\left[\Delta S_U^b(1) - \Delta S_U^b(\infty)\right] \tag{8}$$

The introduction of defects progressively helps nucleation. In the case of Cu–Zn–Al (electronic concentration e.c. = 1.48), the application of expression (8) to the measurements presented in Fig. 9 produces around 11 μJ g^{-1} K^{-1} when $T \approx 260$ K and $\Delta T \approx 4$ K. This is equivalent to around 24 mJ cm^{-3} and the energy necessary to create the corresponding dislocations

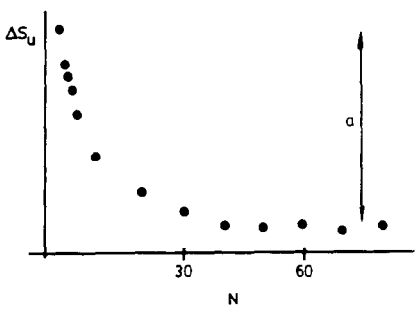

Fig. 9. Entropy production ΔS_U^b (in arbitrary units) versus cycle number. Sample after air quenching; the arrow (a) indicates the change of the entropy production with spontaneous cycling.

TABLE 4

Temperatures and heat quantities involved in calorimetric cycling processes: A, without thermoelasticity; B, with thermoelasticity

	Temperature	Heat absorbed by the sample	Heat absorbed by the bath
A			
β to martensite	$M_s\,(=M_f)$	$Q_{\beta\to m}$	$Q_M\,(=-Q_{\beta\to m})$
Martensite to β	$A_s\,(=A_f)$	$Q_{m\to\beta}$	$Q_A\,(=-Q_{m\to\beta})$
B			
β to martensite	M_s to M_f	$Q_{\beta\to m}$	$Q_M\,(=-Q_{\beta\to m})$
Martensite to β	A_s to A_f	$Q_{m\to\beta}$	$Q_A\,(=-Q_{m\to\beta})$

after 200 cycles is close to 80 mJ cm^{-3} [73] but the temperature rates used in cycling are greater. The results show us that the irreversibilities (driving forces ΔG) associated with burst transformations are close to the energies for creation of dislocations. Furthermore, the description of the heat "burst" (lasting several seconds) is much slower and "gentler" than the mechanical process. Using a "full adiabatic" condition, $\Delta T \approx 14$ K and the driving forces approach 2 J cm^{-3}. This suggests that the entropy production changes are only connected qualitatively to the permanent structural deformation.

Hysteretic behaviour and the second law: the Carnot cycle approach

In order to obtain an entropy balance and a calculation of the equivalent "friction work" associated with spontaneous (external stress free) calorimetrically induced transformations, it is necessary to model the process undergone by the material (see Table 4 and Figs. 10 and 11). In an initial approach, it may be considered that T_0, the theoretical equilibrium temperature of transformation, is $T_0 \approx (M_s + A_f)/2$ and that the heat capacity of martensite and the heat capacity of the β-phase are equal ($c_\beta = c_m$). Mechanical stress-induced transformations with one or more single-variant martensite domains are made at constant temperature (equivalent, in temperature-induced transformation, to the process abcd in Fig. 10 or the reversible transformation bc in Fig. 11). Spontaneous temperature-induced transformations, with a single variant, are related to the process abc'd'a in Fig. 10 or, in a reversible situation, to the process bd in Fig. 11. In order to pass from point c to point d in Fig. 11, a transformation over the martensite–parent phase coexistence line can be made.

Calorimetric observations of spontaneous, stress-free cooling ($\sigma_{ext} = 0$) have revealed complex morphologies produced by the different variants. This results in their representative point d not being able to be related to point c (Fig. 11). With this type of process, points c and d are at external

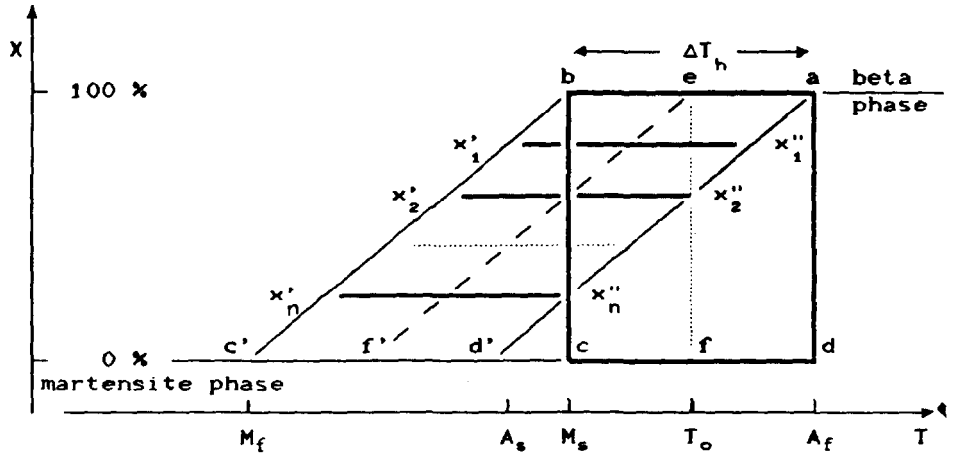

Fig. 10. Schematic hysteretic behaviour in X (% β phase) versus temperature; cycle abcda, phase transformation with hysteresis; cycle abc'd'a, thermoelastic with hysteretic behaviour; aefc', reversible phase transformation (bc in Fig. 11); aef'c', thermoelastic reversible transformation (bd in Fig. 11).

stress zero ($\sigma_{ext} = 0$), and at different temperatures. In order to construct a thermodynamic cycle it is necessary to be able to pass with continuity from one point to another. However, at point c we have a single variant, induced by a very weak stress or by education of the material. At point d we have a heterogeneous system which, by external stress perturbation (from $\sigma = 0$, increasing to $\sigma = \delta\sigma$ and decreasing to the initial value $\sigma = 0$), may become homogeneous (single variant). This shows us that the energy results (or the entropy calculated from eqn. (18)) obtained calorimetrically in

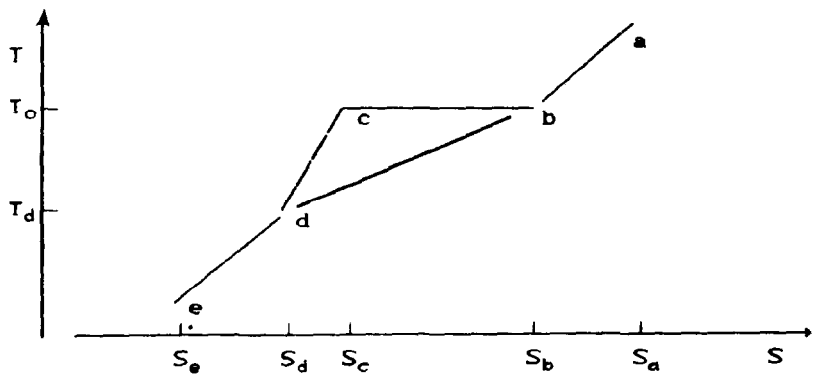

Fig. 11. Schematic temperature–entropy diagram in reversible transformations; ab, cooling β phase; bc, phase transformation at constant temperature ($\beta \rightarrow$ m); bd, "thermoelastic" transformation, cooling and stress-free (equivalent to the idealized spontaneous transformation in calorimetric processes); cd, cooling changing external stress (coexistence between β and martensite phases); de, cooling martensite phase.

spontaneous transformations are not strictly linked to the change of phase to a single variant of martensite.

The friction work in a mechanical stress-induced transformation–re-transformation cycle is obtained directly from $\oint \vec{f}_{ext}\, d\vec{l}$. In order to calculate the fictitious "friction work" associated with temperature-induced transformation, we shall consider only the cycle abcda in Fig. 10. In our case, eqn. (6) reads $|Q_M| = |Q_A|$. The production of entropy $\Delta S^s_U(tb)$ associated with the changes in the thermal baths is

$$\Delta S^s_U(tb) = Q_M/M_s + Q_A/A_f = Q_M(A_f - M_s)/(A_f M_s) \quad (9)$$

The work, W_{CC} (CC ≡ Carnot cycle), which would produce a Carnot machine between A_f and M_s absorbing an amount of heat $|Q_A|$, would be

$$W_{CC} = |Q_A|(A_f - M_s)/A_f = Q_M(A_f - M_s)/A_f \quad (10)$$

If this amount of work is released in the form of heat at temperature M_s, the corresponding entropy production $\Delta S^s_U(CC)$ is

$$\Delta S^s_U(CC) = W_{CC}/M_s = Q_M(A_f - M_s)/(A_f M_s) = \Delta S^s_U(tb) \quad (11)$$

The above expression enables us to define W^{fw}, a fictitious "friction work", in the temperature-induced transformation from

$$W^{fw} \equiv W_{CC} = M_s \Delta S^s_U(CC) = |Q_A|(A_f - M_s)/A_f = Q_M(A_f - M_s)/A_f \quad (12)$$

The fictitious friction work is the work obtained in an equivalent Carnot cycle working from the upper (A_f) to the lower (M_s) temperatures.

The free energy language (see Fig. 12), the Gibbs free energy (the driving force) necessary to overcome the friction terms $\Delta G_{T=M_s}$ and $\Delta G_{T=A_f}$ are defined by

$$\Delta G_{T=M_s} \approx \frac{\partial \Delta G}{\partial T} \Delta T = -(M_s - T_0)\Delta S_{\beta \to m} \quad (13)$$

$$\Delta G_{T=A_f} \approx \frac{\partial \Delta G}{\partial T} \Delta T = -(A_f - T_0)\Delta S_{m \to \beta}$$

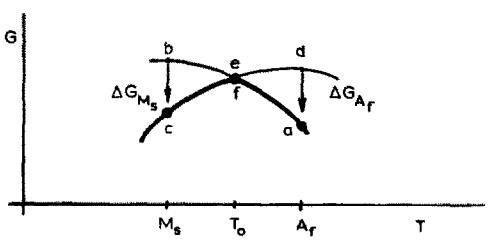

Fig. 12. Gibbs function (parent with only one martensite plate) versus temperature at constant stress (schematic). Coexistence between β and martensite at equilibrium temperature T_0; aefc, reversible transformation path; aebcfda, hysteretic behaviour (type abcda in Fig. 10).

with

$$\Delta S_{\beta\to m} = -\Delta S_{m\to\beta} = S_m - S_\beta = Q_{\beta\to m}/T_0$$

The associated entropy production in a complete thermal cycle is

$$\Delta S_U^G = -\left[\Delta G_{T=M_s}/M_s + \Delta G_{T=A_f}/A_f\right] = Q_M \frac{A_f - M_s}{M_s A_f} \equiv \Delta S_U^s(tb) \qquad (14)$$

ΔS_U^G is, obviously, equal to the $\Delta S_U^s(tb)$ obtained from the heat transferred to (and from) the heat sinks in the calorimetric cycle. The previous analysis shows that the relevant quantities that explain the hysteretic behaviour are, for instance, the entropy production: ΔS_U, ΔS_U^b and ΔS_U^s.

When the hysteresis cycle has thermoelasticity (abc'd'a in Fig. 10), partial cycles should be considered from zones of transformation–retransformation, such as $abx_1'x_1''a$, $x_1''x_1'x_2'x_2''x_1''$, ..., $x_n''x_n'c'd'x_n''$. If the width ΔT_h of the hysteresis cycle is nearly constant, a straightforward (geometric) approach gives us

$$M_s \Delta S_U^s(CC) = W^{fw} \approx 2Q_M \Delta T_h/(A_s + A_f) \qquad (15)$$

If we define "thermal efficiency" $\eta_{th}\%$, from the associated Carnot cycle, by

$$\eta_{th} = 100W^{fw}/Q_M \approx 200\Delta T_h/(A_s + A_f) \qquad (16)$$

immediate information is obtained on the relative importance of the hysteresis cycle from the temperature involved. The values of η_{th} are consistent with those obtained from direct mechanical measurements of the friction cycle. For this, the "mechanical inefficiency" $\eta_m\%$ may be defined as

$$\eta_m = 100 \oint \vec{f}_{ext}\, d\vec{l}/Q_M \qquad (17)$$

For the equivalent cycles (in temperature and stress-induced transformations), the η_{th} and η_m values are practically equal [68,74,75] and hysteretic width dependent: 0.1% in single interface β to β' growing/shrinking, 1% in INSTRON-type measurements, single variant (in spontaneous calorimetric measurements $\approx 3\%$) and 10% in β to 2H measurements. Values of η_{th} recalculated from experimental data in the literature (if available), are shown in Table 2.

From analysis of the elemental cycle bcd in Fig. 11, it is possible to calculate thermoelastic energies, and also to "avoid" the irreversibility of the cycle in order to obtain an approach to the entropy change of the material in its spontaneous transformation, from the relationship

$$\Delta S_{\beta\to m} = \int_{M_s}^{M_f} \frac{\delta Q}{(T - 0.5\Delta T_h)} \qquad (18)$$

which, in the case of Cu–Zn–Al ($\beta \rightarrow \beta'$ transformation) does not differ significantly from the direct value of $\int \delta Q/T$. For $T \approx 300$ K and $0.5\Delta T_h \leq 5$ K, the $\Delta S_{\beta \rightarrow m}$ differs from $\int \delta Q/T$ by approx. 2%. Speakly strictly, $\int \delta Q/T$ is only connected with the entropy changes in the thermal baths. Obviously, a transformation to a single variant does not have the difficulties mentioned above: its temperature range is much smaller because it is only affected by intrinsic thermoelasticity, but current reliability of the results is poor. There is considerable uncertainty in the calculation of the transformed mass and some metastabilities are observed. Similarly, direct calorimetric tests on stress–strain systems are still inaccurate.

CONCLUSIONS

The development of the experimental systems of HRTA with automatic, strictly reproducible programmings has made it possible to increase our understanding of the processes that occur in memory alloys. For this, the Peltier effect and a rigorous programming based on the analyses of the dynamic behaviour of the device have been used. From basic HRTA equipment, other auxiliary techniques have been adapted to analyse transformation/retransformation processes with high resolution: thermomicroscopy, electrical resistance, heat conduction calorimetry, stress–strain studies, etc.

The observations have shown that HRTA studies in shape-memory alloys are very sensitive to minor structural changes. This is easily demonstrated when reproducible behaviour and, where appropriate, evolution of the material due to changes in the atomic order and/or creation of defects caused by the transformation itself, are obtained. The relevance of the processes of nucleation and growth in the hysteresis cycle is clearly established. In this respect, the intrinsic thermoelasticity associated with the concentration of dislocations is of highest importance in ensuring memory effect.

Thermodynamic analysis establishes the strict coherence between the friction obtained in entropic terms from the width of the hysteresis cycle, determined calorimetrically, and the friction energy measured directly in the stress–strain diagram. Its values are around 1% in the spontaneous transformation at 18R ($\beta \rightarrow \beta'$) and around 10% in the transformation at 2H ($\beta \rightarrow \gamma'$). Obviously, recent thermodynamic interpretations using thermodynamic potentials and dissipative terms, identifying (in thermal cycles and without external stresses) the friction work with the global heat measured, are wrong. The relevant quantity in the thermal cycles is the entropy production related to the hysteresis width. In addition, the calorimetric thermograms, considered to be a result of the entropy of the "burst processes", are consistent with the creation of dislocations.

ACKNOWLEDGEMENTS

Dr. Amengual (UIB-Spain), Dr. A. Isalgue (ETSAB/UPC-Spain) and Dr. Lovey (CAB-Argentina) are gratefully acknowledged for their help in the experimental measurements and for their enlightening discussions. Contacts between the two countries are supported by DGICYT (H.T., sabatic program) and Univ. Provence (V.T. Associate Professor). V.T. acknowledges the Lagrange Group (L.A. Garcia-Ramos) for aid in the optimal choice of computer hardware. Experimental research in Spain is carried out in the framework of the CICYT project MAT89-0407-C03.

REFERENCES

1 V. Torra (Ed.), Science and Technology in Shape Memory Alloys, Proc. COMETT Course 1989, Barcelona, Spain, Universitat de les Illes Balears, Spain, 1989.
2 B.C. Muddle (Ed.), Martensitic Transformations I and II, Proc. ICOMAT 89, Materials Science Forum, Vol. 56–58, Trans. Tech. Publications, Zürich, 1990.
3 I. Tamma (Ed.), Proc. ICOMAT 86, The Japan Institute of Metals, Sendai, Japan, 1987.
4 E. Hornbogen and N. Jost (Eds.), The Martensitic Transformation in Science and Technology, DGM, Oberursel, Germany, 1989.
5 Proc. COMETT II Course, Technologie et Mise en Oeuvre des Alliages à Memoire de Forme, IMAGO, La Ciotat, France, 1991.
6 G.W. Lorimer (Ed.), Proc. Conf. Phase Transformations 87, The Institute of Metals, Cambridge, UK, 1988.
7 M. Ahlers, Prog. Mater. Sci., 30 (1986) 135–186.
8 A. Caneiro and M. Chandrasekaran, Scr. Metall., 22 (1988) 1797–1800.
9 W. Zongguo and Y. Dazhi, Scr. Metall., 22 (1988) 1245–1249.
10 L. Li, A. Aernoudt and L. Delaey, Scr. Metall., 22 (1988) 1435–1440.
11 J.M. Guilemany and F.J. Gil; Mater. Res. Bull., 25 (1990) 1325–1332.
12 D.Z. Yang, M. Zhu, M. Qi and G.B. Li, Scr. Metall., 20 (1986) 1717–1720.
13 L. Delaey, J. Ortin and J.V. Humbeeck, ref. 6, pp. 60–66.
14 N. Ono and H. Shimanuki, Scr. Metall. Mater., 24 (1990) 2269–2272.
15 M. de Graqef and L. Delaey, ref. 2. pp. 423–428.
16 D.G. Maeder and M. Droz, ref. 2, pp. 119–124.
17 I. Takahashi and T. Suzuki, ref. 2, pp. 125–130.
18 E. Patoor, A. Eberhardt and M. Berveiller, ref. 4, pp. 133–140.
19 R. Stalmans, J.V. Humbeeck and L. Delaey, ref. 4, pp. 207–212.
20 I. Muller and H. Xu, Acta Metall. Mater., 39 (1991) 263–271.
21 A. Planes, J.L. Macqueron and J. Ortin, Philos. Mag. Lett., 57 (1988) 291–298.
22 F.C. Lovey, J. Ortin and V. Torra, Phys. Lett. A, 121 (1987) 353–356.
23 A. Amengual, F. Garcias, F. Marco, C. Segui and V. Torra, Acta Metall., 36(8) (1988) 2329–2334.
24 M. Rodriguez de Rivera, F. Socorro, J.P. Dubés, H. Tachoire and V. Torra, Thermochim. Acta, 150 (1989) 11–25.
25 A. Amengual, F. Marco, M. Rodriguez de Rivera and V. Torra, Thermochim. Acta, 188 (1991) 63–76.
26 H. Tachoire, J.L. Macqueron and V. Torra, in M.A.V. Ribeiro da Silva (Ed.), Thermochemistry and Its Applications to Chemical and Biochemical Systems, NATO ASI Series C 119, D. Reidel Publishing Co., Dordrecht, 1984, pp. 77–126.

27 W. Zielenkiewicz (Ed.), Thermokinetics. Signal processing in Calorimetric Systems, Ossolineum, Warsaw, 1990.
28 H. Tachoire, J.L. Macqueron and V. Torra, Thermochim. Acta, 105 (1986) 333–367.
29 H. Tachoire and V. Torra, Can. J. Chem., 67 (1989) 983–990.
30 P. Thuillier and J.C. Belloc, Mathematiques – Analyse 3, Masson, Paris, 1989, pp. 181–194.
31 J.R. Rodriguez, C. Rey, V. Perez-Villar, V. Torra, J. Ortin and J. Viñals, Thermochim. Acta, 63 (1983) 331–339.
32 A. Amengual and V. Torra, J. Phys. E: Sci. Instrum., 22 (1989) 433–437.
33 A. Amengual, V. Torra, A. Isalgué, and F. Marco, Thermochim. Acta, 155 (1989) 115–134.
34 V. Torra and H. Tachoire, J. Therm. Anal., 36 (1990) 1545–1577.
35 V. Torra, V.R. Torra, A. Isalgue and F. Marco, Thermochim. Acta, 200 (1992) 413–426.
36 C. Picornell, C. Segui, V. Torra, J. Hernáez and C. López del Castillo, Thermochim. Acta, 91 (1985) 311–320.
37 C. Picornell, C. Segui, V. Torra, C. Auguet, Ll. Mañosa, E. Cesari and R. Rapacioli, Thermochim. Acta, 106 (1986) 209–217.
38 G. Guenin, J.L. Macqueron, M. Mantel, C. Auguet, E. Cesari, Ll. Mañosa, A. Planes, C. Picornell, C. Segui, J. Ortin and V. Torra, ref. 3, pp. 794–799.
39 A. Amengual, Ll. Mañosa, F. Marco, C. Picornell, C. Segui and V. Torra, Thermochim. Acta, 116 (1987) 195–208.
40 N. Nakanishi, T. Shigematsu, M. Yasuoka, H. Oshima and S. Miura, ref. 3, pp. 210–215.
41 A. Steiner, R. Gotthard and D.G. Maeder, ref. 3, pp. 216–221.
42 F.C. Lovey, E. Cesari, V. Torra and J.M. Guilemany, Mater. Lett., 5 (1987) 159–162.
43 C. Picornell, C. Segui, V. Torra, F.C. Lovey and R. Rapacioli, Thermochim. Acta, 113 (1987) 171–183.
44 A. Planes, J. Viñals and V. Torra, Philos. Mag. A, 48 (1983) 501–508.
45 J. Viñals, V. Torra, A. Planes and J.L. Macqueron, Philos. Mag. A, 50 (1984) 653–666.
46 A. Planes, R. Romero and M. Ahlers, Acta Metall., 38 (1990) 757–763.
47 A. Amengual, F.C. Lovey and V. Torra, Scr. Metall., 24 (1990) 2241–2246.
48 A. Amengual and V. Torra, Thermochim. Acta, 198 (1992) 267–278.
49 M. Chandrasekaran, L. Cooreman, J.V. Humbeeck and L. Delaey, Scr. Metall., 23 (1989) 237–239.
50 X. Duan and W.M. Stobbs, Scr. Metall., 23 (1989) 441–445.
51 T. Suzuki, R. Kojima, Y. Fujii and A. Nagasawa, Acta Metall., 37 (1989) 163–168.
52 C. Cooreman, J.V. Humbeeck and L. Delaey, Acta Metall., 38 (1990) 2663–2666.
53 F.C. Lovey, A. Amengual, V. Torra and M. Ahlers, Philos. Mag. A, 61 (1990) 159–165.
54 F.C. Lovey, A. Amengual and V. Torra, Philos. Mag. A, 64 (1991) 787–796.
55 R.J. Salzbrenner and M. Cohen, Acta Metall., 27 (1979) 739–748.
56 J. Ortin, Thermochim. Acta, 121 (1987) 397–412.
57 J. Ortin and A. Planes, Acta Metall., 36 (1988) 1873–1889.
58 J. Ortin and A. Planes, Acta Metall., 37 (1989) 1433–1441.
59 J. Ortin and A. Planes, ref. 4, pp. 75–82.
60 J. Ortin and A. Planes, ref. 2, pp. 139–144.
61 A. Planes, J.L. Macqueron, R. Rapacioli and G. Guenin, Philos. Mag. A, 61 (1990) 221–231.
62 C. Auguet, E. Cesari, R. Rapacioli and Ll. Mañosa, Scr. Metall., 23 (1989) 579–583.
63 C. Auguet, E. Cesari and Ll. Mañosa, J. Phys. D: Appl. Phys., 22 (1989) 1712–1720.
64 C. Picornell, M. Sade and E. Cesari, Scr. Metall., 23 (1989) 371–376.
65 C.M. Friend, J. Ortin, A. Planes, Ll. Mañosa and M. Yoshikawa, Scr. Metall. Mater., 24 (1990) 1641–1645.
66 J. Pons, E. Cesari and M. Roca, Mater. Lett., 9 (1990) 542–546.

67 C. Segui, E. Cesari and J.V. Humbeeck, Mater. Trans. Jpn. Inst. Metals, 31 (1990) 375–380.
68 J.L. Pelegrina, Ph.D. Thesis, 1990, Instituto Balseiro, CAB, Bariloche, Argentina.
69 S.C. Mraw, Rev. Sci. Instrum., 53 (1982) 228–231.
70 C. Sandu and R.K. Singh, Thermochim. Acta, 159 (1990) 267–298.
71 E. Urbanovici and E. Segal, Thermochim. Acta, 159 (1990) 369–372.
72 J. Ortin, V. Torra and H. Tachoire, Thermochim. Acta, 121 (1987) 333–342.
73 J. Pons, F.C. Lovey and E. Cesari, Acta Metall. Mater., 38 (1990) 2733–2740.
74 M. Ahlers, F.C. Lovey, J.L. Pelegrina, A. Amengual and V. Torra, unpublished results, 1990.
75 A. Amengual, Ph.D. Thesis, 1990, Physics Dept., Univ. Illes Balears, Spain.